Journal of Fluids and Structures (2002) **16**(1), 53–70
doi:10.1006/jfls.2001.0409, available online at http://www.idealibrary.com on IDEAL®

INITIALLY TENSIONED ORTHOTROPIC CYLINDRICAL SHELLS CONVEYING FLUID: A VIBRATION ANALYSIS

Y. L. Zhang

Department of Chemical Engineering & Chemical Technology
Imperial College of Science, Technology and Medicine
Prince Consort Road, London SW7 2BY, U.K.

J. M. Reese

Department of Mechanical Engineering, King's College London
Strand, London WC2R 2LS, U.K.

AND

D. G. Gorman

Department of Mechanical Engineering, University of Strathclyde
James Weir Building, Montrose Street, Glasgow G1 XXJ, U.K.

(Received 28 July 2000, and in final form 6 June 2001)

A linear analysis of the vibratory behaviour of initially tensioned orthotropic circular cylindrical shells conveying a compressible inviscid fluid is presented. The model is based on the three-dimensional nonlinear theory of elasticity and the Eulerian equations. A nonlinear strain–displacement relationship is employed to derive the geometric stiffness matrix due to initial stresses and hydrostatic pressures. Frequency-dependent fluid mass, damping and stiffness matrices associated with inertia, Coriolis and centrifugal forces, respectively, are derived through the fluid–structure coupling condition. The resulting equation governing the vibration of fluid-conveying shells is solved by the finite element method. The free vibration of initially tensioned orthotropic cylindrical shells conveying fluid is investigated; numerical examples are given and discussed.

1. INTRODUCTION

Numerous papers on the dynamic behaviour of cylindrical shells conveying fluid have been published, particularly for shells made of isotropic materials [e.g., Païdoussis & Mateescu (1987)]; an excellent review is given by Chen (1987). In examining the dynamics of fluid-conveying shells, it is important to be able to estimate natural frequencies and to establish the critical flow velocity at which large displacements develop. Païdoussis & Denise (1972) theoretically accounted for, and experimentally confirmed, the phenomenon that thin isotropic cylindrical shells conveying fluid, either cantilevered or clamped at both ends, lose stability by flutter when the internal flow velocity exceeds a certain critical value. Weaver & Unny (1973) investigated the stability of a fluid-conveying isotropic cylinder, simply supported at both ends. An experimental study of annular-flow-induced instabilities of

0889–9746/02/010053 + 18 $35.00/0

cylindrical shells was completed by Chebair *et al.* (1989), who investigated the effect of flow velocity on the natural frequency of a cylindrical shell within a coaxial rigid cylindrical pipe, and thereby predicted that inner pressurization of the shell stabilizes the system. However, with increasing use of composite materials (due to their light weight and high specific strength) more and more attention is now being paid to orthotropic cylindrical shells (Sharma *et al.* 1996; Ramasamy & Ganesan 1999), but, to the authors' knowledge, there has been no work reported on the vibration of initially tensioned orthotropic shells conveying fluid.

Païdoussis *et al.* (1985) investigated the stability of axially stressed isotropic coaxial cylindrical shells with internal and annular flow. The effect of viscous forces, which were determined by means of upstream pressurization of the flow and skin friction on the shell surfaces, was also studied. Jain (1974) investigated the dynamic problems of fluid-filled orthotropic cylindrical shells. Theoretical solutions of the free vibrations of orthotropic cylindrical shells conveying fluid have also been obtained with the use of the Ritz variational method and potential flow by using Bessel functions (Shang & Lei 1988). The exact solution of nonaxisymmetric free vibrations of simply supported orthotropic cylindrical shells containing fluid has previously been derived by using displacement separation and orthogonal series expansion (Chen *et al.* 1997). Sharma *et al.* (1998) also developed an analytical solution of the free-vibration response of multilayered orthotropic fluid-filled circular cylindrical shells by using the theory of thin shells and potential flow theory. However, most of these investigations were confined to orthotropic shells containing quiescent or flowing fluid (Chang & Chiou 1995) in which the solution for the fluid domain is obtained as a potential flow by using Bessel functions. Bradford & Dong (1978) illustrated the influence of axial prestresses on the free vibration of a three-layer composite and a sandwich cylinder. Sivadas (1995) analysed the effect of prestresses and internal/external pressures on the natural frequencies of prestressed thick circular conical composite shells. Lakis & Selmane (1997) conducted a hybrid-finite-element analysis of the free vibration of anisotropic cylindrical shells subjected to a flowing fluid by using the Sanders theory of thin shells and potential flow theory; the exact displacement function was derived from the equilibrium equations of the empty shell without initial stresses (e.g., initial axial stresses or initial circumferential stresses within the shell due to hydrostatic pressures).

In this paper, a new finite-element formulation for initially tensioned orthotropic cylindrical shells conveying compressible inviscid fluid is presented on the basis of a three-dimensional theory of elasticity and the Euler equations. The hydrodynamic pressure is derived from the Euler equation and the dynamic coupling conditions. A nonlinear strain–displacement relationship is deployed for deriving the geometric stiffness matrix, although the subsequent vibratory analysis is fully linear. Numerical examples of transversely isotropic cylindrical shells in the absence of and containing quiescent and flowing fluid, and initially tensioned orthotropic cylindrical shells in the absence of and conveying fluid are presented and discussed.

2. FORMULATION OF THE PROBLEM

2.1. The Shell Equation

Consider an initially tensioned circular cylindrical shell with internal and external diameters d and D respectively, a thickness h, and a length L. The shell material is assumed to be orthotropic and linearly elastic. The dynamic problem of compressible inviscid fluid-conveying initially uniaxially stretched cylindrical shells may be formulated in a cylindrical

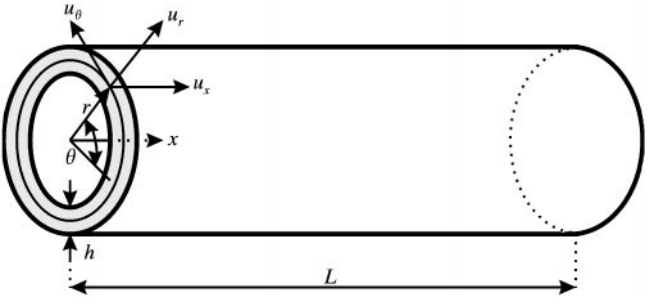

Figure 1. Schematic diagram of the model.

polar coordinate system (r, θ, x) as shown in Figure 1. The fluid flow in the shell is steady. The detailed derivation of the dynamic equations of the coupled fluid–structure interaction is given by Zhang *et al.* (2001), but the approach is briefly summarized below for completeness, with the novel additional considerations of fluid compressibility, initial tension and orthotropic material properties. The cylindrical polar coordinate system is chosen with the x-axis along the axis of the shell, and r and θ along the radial and circumferential directions, respectively.

The components of the displacement are denoted by u_x, u_θ and u_r in the axial, tangential and radial directions, respectively. The dynamic displacement vector in the coordinate system is expressed as (all symbols are listed for convenience in Appendix A):

$$\mathbf{u} = \begin{Bmatrix} u_x \\ u_\theta \\ u_r \end{Bmatrix} \equiv \begin{Bmatrix} u_x(x, \theta, r, t) \\ u_\theta(x, \theta, r, t) \\ u_r(x, \theta, r, t) \end{Bmatrix}. \tag{1}$$

For the local material principal axes 1–2–3 coinciding with the global cylindrical coordinates, the constituent relationship between the strain and stress vector for an orthotropic material, obeying the generalized Hook's law, is given by (Lekhnitskii 1963)

$$\begin{aligned}
\varepsilon_{xx} &= \frac{1}{E_{xx}}\sigma_{xx} - \frac{\nu_{\theta x}}{E_{\theta\theta}}\sigma_{\theta\theta} - \frac{\nu_{rx}}{E_{rr}}\sigma_{rr}, \qquad \gamma_{x\theta} = \frac{1}{G_{x\theta}}\tau_{x\theta}, \\
\varepsilon_{\theta\theta} &= -\frac{\nu_{x\theta}}{E_{xx}}\sigma_{xx} + \frac{1}{E_{\theta\theta}}\sigma_{\theta\theta} - \frac{\nu_{r\theta}}{E_{rr}}\sigma_{rr}, \qquad \gamma_{\theta r} = \frac{1}{G_{\theta r}}\tau_{\theta r}, \\
\varepsilon_{rr} &= -\frac{\nu_{xr}}{E_{xx}}\sigma_{xx} - \frac{\nu_{\theta r}}{E_{\theta\theta}}\sigma_{\theta\theta} + \frac{1}{E_{rr}}\sigma_{rr}, \qquad \gamma_{rx} = \frac{1}{G_{rx}}\tau_{rx},
\end{aligned} \tag{2}$$

where $E_{xx}\nu_{\theta x} = E_{\theta\theta}\nu_{x\theta}$, $E_{xx}\nu_{rx} = E_{rr}\nu_{xr}$, and $E_{rr}\nu_{\theta r} = E_{\theta\theta}\nu_{r\theta}$.

On considering a shell subjected to initial tensions, equations (2) can be rewritten in matrix form:

$$\boldsymbol{\sigma} = \{\sigma^0_{xx}, \sigma^0_{\theta\theta}, \sigma^0_{rr}, \tau^0_{x\theta}, \tau^0_{\theta r}, \tau^0_{rx}\}^{\mathrm{T}} + \{\sigma_{xx}, \sigma_{\theta\theta}, \sigma_{rr}, \tau_{x\theta}, \tau_{\theta r}, \tau_{rx}\}^{\mathrm{T}} = \mathbf{D}\boldsymbol{\varepsilon}, \tag{3}$$

where $\mathbf{D}$ represents the orthotropic shell stress–strain matrix in the global coordinate system, i.e.,

$$\mathbf{D} = \begin{bmatrix} D_{11} & D_{12} & D_{13} & 0 & 0 & 0 \\ D_{12} & D_{22} & D_{23} & 0 & 0 & 0 \\ D_{13} & D_{23} & D_{33} & 0 & 0 & 0 \\ 0 & 0 & 0 & D_{44} & 0 & 0 \\ 0 & 0 & 0 & 0 & D_{55} & 0 \\ 0 & 0 & 0 & 0 & 0 & D_{66} \end{bmatrix}, \tag{4}$$

where components D_{ij} in $\mathbf{D}$ are given in Appendix B. For an isotropic material, this constitutive relationship matrix takes the form

$$\mathbf{D} = \frac{E}{(1+\nu)(1-2\nu)} \begin{bmatrix} 1-\nu & \nu & \nu & 0 & 0 & 0 \\ \nu & 1-\nu & \nu & 0 & 0 & 0 \\ \nu & \nu & 1-\nu & 0 & 0 & 0 \\ 0 & 0 & 0 & \frac{1}{2}(1-2\nu) & 0 & 0 \\ 0 & 0 & 0 & 0 & \frac{1}{2}(1-2\nu) & 0 \\ 0 & 0 & 0 & 0 & 0 & \frac{1}{2}(1-2\nu) \end{bmatrix}. \tag{5}$$

For a geometrically nonlinear analysis, the strain vector in the cylindrical polar coordinate (x, θ, r) system is given by

$$\boldsymbol{\varepsilon} = \boldsymbol{\varepsilon}_0 + \boldsymbol{\varepsilon}_{\mathrm{L}} + \boldsymbol{\varepsilon}_{\mathrm{NL}} = \boldsymbol{\varepsilon}_0 + \{\varepsilon_{xx},\ \varepsilon_{\theta\theta},\ \varepsilon_{rr},\ \gamma_{x\theta},\ \gamma_{\theta r},\ \gamma_{rx}\}^{\mathrm{T}}, \tag{6}$$

where $\boldsymbol{\varepsilon}_{\mathrm{L}}$ and $\boldsymbol{\varepsilon}_{\mathrm{NL}}$ are defined by (Zienkiewicz & Taylor 1991)

$$\boldsymbol{\varepsilon}_{\mathrm{L}} = \begin{Bmatrix} u_{x,x} \\ \frac{1}{r}(u_{\theta,\theta} + u_r) \\ u_{r,r} \\ \frac{1}{r}u_{x,\theta} + u_{\theta,x} \\ \frac{1}{r}(u_{r,\theta} + u_\theta) - u_{\theta,r} \\ u_{r,x} + u_{x,r} \end{Bmatrix}, \qquad \boldsymbol{\varepsilon}_{\mathrm{NL}} = \begin{Bmatrix} \frac{1}{2}(u_{x,x}^2 + u_{\theta,x}^2 + u_{r,x}^2) \\ \frac{1}{2r^2}[(u_{r,\theta} - u_\theta)^2 + (u_{\theta,\theta} + u_x)^2 + (u_{x,\theta})^2] \\ \frac{1}{2}(u_{x,r}^2 + u_{\theta,r}^2 + u_{r,r}^2) \\ \frac{1}{r}[(u_{r,\theta} - u_\theta)u_{r,x} + (u_{\theta,\theta} + u_r)u_{\theta,x} + u_{x,\theta}u_{x,x}] \\ \frac{1}{r}[(u_{r,\theta} - u_\theta)u_{r,r} + (u_{\theta,\theta} + u_r)u_{\theta,r} + u_{x,\theta}u_{x,r} \\ \frac{1}{r}(u_{x,r}u_{x,x} + u_{\theta,r}u_{\theta,x} + u_{r,r}u_{r,x})] \end{Bmatrix}. \tag{7}$$

Upon setting $\boldsymbol{\beta} = \{\beta_1,\ \beta_2,\ \beta_3,\ \beta_4,\ \beta_5,\ \beta_6,\ \beta_7,\ \beta_8,\ \beta_9\}^{\mathrm{T}}$, the linear and nonlinear parts of the Green strain vector can be rewritten as

$$\boldsymbol{\varepsilon}_{\mathrm{L}} = \mathbf{H}_1\boldsymbol{\beta} \text{ and } \boldsymbol{\varepsilon}_{\mathrm{NL}} = \tfrac{1}{2}\mathbf{H}_2\boldsymbol{\beta}, \tag{8}$$

where $\mathbf{H}_1$, $\mathbf{H}_2$ and $\boldsymbol{\beta}$ are given in Appendix B.

At fluid–structure interfaces, surface traction exerted on the shell wall can be separated into two parts, one due to steady hydrostatic pressures and the other due to hydrodynamic pressures. The strain energy of the shell and the energy of external forces on the shell are given, respectively, by

$$V(\mathbf{u}) = \frac{1}{2}\int_{\Omega_{\mathrm{t}}} \boldsymbol{\varepsilon}^{\mathrm{T}}\mathbf{D}\boldsymbol{\varepsilon}\,\mathrm{d}\Omega_{\mathrm{t}} \text{ and } W(\mathbf{u}) = \int_{\Omega_{\mathrm{t}}} \mathbf{u}^{\mathrm{T}}\boldsymbol{\rho}_{\mathrm{t}}\ddot{\mathbf{u}}\,\mathrm{d}\Omega_{\mathrm{t}} - \int_{\Gamma_{\mathrm{t}}} \mathbf{u}^{\mathrm{T}}(\mathbf{p}_{\mathrm{t}} + \mathbf{q}_{\mathrm{t}})\,\mathrm{d}\Gamma_{\mathrm{t}}, \tag{9}$$

where the dot represents the derivative with respect to time.

The total potential energy of the shell is therefore given by

$$\Pi = V(\mathbf{u}) + W(\mathbf{u}) = \frac{1}{2}\int_{\Omega_t} \boldsymbol{\varepsilon}^{\mathrm{T}}\mathbf{D}\boldsymbol{\varepsilon}\,\mathrm{d}\Omega_t + \int_{\Omega_t} \mathbf{u}^{\mathrm{T}}\boldsymbol{\rho}_t\ddot{\mathbf{u}}\,\mathrm{d}\Omega_t - \int_{\Gamma_t} \mathbf{u}^{\mathrm{T}}(\mathbf{p}_t + \mathbf{q}_t)\,\mathrm{d}\Gamma_t. \tag{10}$$

Applying the d'Alembert principle (Bittnar & Sejnoha 1996), the following equation can be obtained:

$$\delta\Pi = \delta V(\mathbf{u}) + \delta W(\mathbf{u}) = \int_{\Omega_t} \delta\boldsymbol{\varepsilon}^{\mathrm{T}}\mathbf{D}\boldsymbol{\varepsilon}\,\mathrm{d}\Omega_t + \int_{\Omega_t} \delta\mathbf{u}^{\mathrm{T}}\boldsymbol{\rho}_t\ddot{\mathbf{u}}\mathrm{d}\Omega_t - \int_{\Gamma_t} \delta\mathbf{u}^{\mathrm{T}}(\mathbf{p}_t + \mathbf{q}_t)\,\mathrm{d}\Gamma_t = 0. \tag{11}$$

2.2. The Fluid Equation

Consider an isotropic and compressible inviscid fluid occupying a region Ω_f within a cylindrical shell with boundary Γ_f, and neglect the fluid gravity force. It is assumed that the lateral pressure which induces the circumferential stress is constant directional: the direction and magnitude per unit original area remain unchanged during deformation. It is also assumed that perturbation originating in the shell oscillation is small at both inlet and outlet of the shell and so can be neglected. The present analysis of the inviscid fluid flow in the oscillating shell is based on the Eulerian equation in the cylindrical polar coordinate system (r, θ, x), viz.

$$\dot{\mathbf{v}} + \mathbf{v}\cdot\nabla\mathbf{v} = -(1/\rho_f)\nabla p \quad \text{in } \Omega_f, \tag{12}$$

and on the continuity equation

$$\nabla\cdot\mathbf{v} = \dot{p}/K \quad \text{in } \Omega_f. \tag{13}$$

Combining equations (12) and (13) we obtain the following equation:

$$\nabla^2 p - (1/a_f^2)\ddot{p} + \rho_f\nabla\cdot(\mathbf{v}\cdot\nabla\mathbf{v}) = 0 \quad \text{in } \Omega_f. \tag{14}$$

2.3. Boundary Conditions

The motion of the shell wall and fluid are fully coupled by velocities, accelerations and pressures normal to the fluid–structure interface. Restrictions are added so that the fluid particles adhere normal to the fluid–structure interface, i.e.,

$$\mathbf{n}\cdot(\mathrm{d}\mathbf{u}/\mathrm{d}t - \mathbf{v}) = \mathbf{n}\cdot(\dot{\mathbf{u}} + U\mathbf{u}_{,s} - \mathbf{v}) = 0 \quad \text{on } \Gamma_t \cap \Gamma_f, \tag{15a}$$

$$\mathbf{n}\cdot(\mathrm{d}^2\mathbf{u}/\mathrm{d}t^2 - \mathrm{d}\mathbf{v}/\mathrm{d}t) = \mathbf{n}\cdot[\ddot{\mathbf{u}} + 2U\dot{\mathbf{u}}_{,s} + U^2\mathbf{u}_{,ss} - (\mathbf{v} + \mathbf{v}\cdot\nabla\mathbf{v})] = 0 \quad \text{on } \Gamma_t \cap \Gamma_f, \tag{15b}$$

where $\mathrm{d}/\mathrm{d}t$ and $\mathrm{d}^2/\mathrm{d}t^2$ are the first- and second-order material derivatives, respectively; $\mathbf{u}_{,s} \equiv \partial\mathbf{u}/\partial s$; $\mathrm{d}s = [(\mathrm{d}x)^2 + (r\mathrm{d}\theta)^2 + (\mathrm{d}r)^2]^{1/2}$. Given the assumption that perturbations originating from the shell oscillation at both inlet and outlet of the shell are negligible, the following kinematic conditions at the inlet and outlet of the shell are imposed:

$$\mathrm{d}\mathbf{v}/\mathrm{d}t = 0, \quad \text{at } x = 0 \text{ and } L. \tag{15c}$$

In addition to the kinematic boundary conditions, continuity of traction at the fluid–shell interfaces and restriction at inlet and outlet of the shell are imposed, i.e.,

$$(\mathbf{p}_t + \mathbf{p}_f) = \mathbf{0} \quad \text{on } \Gamma_t \cap \Gamma_f, \tag{16a}$$

$$\mathbf{n} \cdot \mathrm{d}\mathbf{v}/\mathrm{d}t = -(1/\rho_\mathrm{f})(\partial p/\partial n) \quad \text{on } \Gamma_\mathrm{t} \cap \Gamma_f, \tag{16b}$$

$$\mathrm{d}\mathbf{v}/\mathrm{d}t = -(1/\rho_\mathrm{f})\nabla p \quad \text{at } x = 0 \text{ and } L. \tag{16c}$$

3. METHOD OF SOLUTION

3.1. Shell Domain

The variables $\mathbf{u}(x, \theta, r, t)$ in equation (11) are expanded isoparametrically. The shell displacement field and its variation, $\delta\mathbf{u}(x, \theta, r, t)$, are approximated by

$$\mathbf{u}(x, \theta, r, t) = \begin{Bmatrix} u_x \\ u_\theta \\ u_r \end{Bmatrix} = \begin{Bmatrix} \mathbf{N}_\mathrm{t}\,\bar{\mathbf{u}}_x \\ \mathbf{N}_\mathrm{t}\,\bar{\mathbf{u}}_\theta \\ \mathbf{N}_\mathrm{t}\,\bar{\mathbf{u}}_r \end{Bmatrix} = \mathbf{N}_\mathrm{T}\bar{\mathbf{u}},$$

$$\delta\mathbf{u}(x, \theta, r, t) = \begin{Bmatrix} \delta u_x \\ \delta u_\theta \\ \delta u_r \end{Bmatrix} = \begin{Bmatrix} \delta(\mathbf{N}_\mathrm{t}\,\bar{\mathbf{u}}_x) \\ \delta(\mathbf{N}_\mathrm{t}\bar{\mathbf{u}}_\theta) \\ \delta(\mathbf{N}_\mathrm{t}\bar{\mathbf{u}}_r) \end{Bmatrix} = \delta\bar{\mathbf{u}}^\mathrm{T}\mathbf{N}_\mathrm{T}^\mathrm{T}, \tag{17}$$

which are continuous. Here $\bar{\mathbf{u}}$ is the nodal displacement vector, i.e., $\bar{\mathbf{u}} = \{\bar{\mathbf{u}}_x, \bar{\mathbf{u}}_\theta, \bar{\mathbf{u}}_r\}^\mathrm{T}$; $\mathbf{N}_\mathrm{t}$ is the shape-function matrix; $\mathbf{N}_\mathrm{T}$ is the assembled shape-function matrix, given in Appendix B. Upon setting $\mathrm{d}\boldsymbol{\beta} = \mathbf{G}\mathrm{d}\bar{\mathbf{u}}$, equation (8) can be rewritten in variational form as

$$\mathrm{d}\boldsymbol{\varepsilon}_\mathrm{L} = \mathbf{H}_1\mathbf{G}\mathrm{d}\bar{\mathbf{u}} = \mathbf{B}_\mathrm{L}\mathrm{d}\bar{\mathbf{u}}, \quad \text{and } \mathrm{d}\boldsymbol{\varepsilon}_\mathrm{NL} = \mathbf{H}_2\mathbf{G}\mathrm{d}\bar{\mathbf{u}} = \mathbf{B}_\mathrm{NL}\,\mathrm{d}\bar{\mathbf{u}}. \tag{18}$$

In the above, the linear strain–displacement matrix, $\mathbf{B}_\mathrm{L}$, the nonlinear strain–displacement matrix, $\mathbf{B}_\mathrm{NL}$, and $\mathbf{G}$ are given in Appendix B.

The standard discretization processes result in the form

$$\int_{\Omega_\mathrm{t}} \mathbf{N}_\mathrm{T}^\mathrm{T}\boldsymbol{\rho}_\mathrm{t}\mathbf{N}_\mathrm{T}\ddot{\bar{\mathbf{u}}}\,\mathrm{d}\Omega_\mathrm{t} + \int_{\Omega_\mathrm{t}} \mathbf{B}_\mathrm{L}^\mathrm{T}\mathbf{D}\mathbf{B}_\mathrm{L}\bar{\mathbf{u}}\,\mathrm{d}\Omega_\mathrm{t} + \int_{\Omega_\mathrm{t}} (\mathbf{B}_\mathrm{L}^\mathrm{T}\mathbf{D}\mathbf{B}_\mathrm{NL} + \mathbf{B}_\mathrm{NL}^\mathrm{T}\mathbf{D}\mathbf{B}_\mathrm{L} + \mathbf{B}_\mathrm{NL}^\mathrm{T}\mathbf{D}\mathbf{B}_\mathrm{NL})\bar{\mathbf{u}}\,\mathrm{d}\Omega_\mathrm{t}$$
$$+ \int_{\Omega_\mathrm{t}} \mathbf{G}^\mathrm{T}\mathbf{S}\mathbf{G}\bar{\mathbf{u}}\,\mathrm{d}\Omega_\mathrm{t} + \int_{\Omega_\mathrm{t}} \mathbf{B}_\mathrm{L}^\mathrm{T}\mathbf{D}\boldsymbol{\varepsilon}^0\,\mathrm{d}\Omega_\mathrm{t} - \int_{\Gamma_\mathrm{t}} \mathbf{N}_\mathrm{T}^\mathrm{T}\mathbf{q}_\mathrm{t}\mathrm{d}\Gamma_\mathrm{t} - \int_{\Gamma_\mathrm{t}} \mathbf{N}_\mathrm{T}^\mathrm{T}\mathbf{p}_\mathrm{t}\,\mathrm{d}\Gamma_\mathrm{t} = 0, \tag{19}$$

where the matrices $\mathbf{G}$ and $\mathbf{S}$ are given in Appendix B.

Equation (19) can be rewritten in the following form:

$$\mathbf{m}_\mathrm{t}\ddot{\bar{\mathbf{u}}} + (\mathbf{k}_{\mathrm{t(L)}} + \mathbf{k}_{\mathrm{t(NL)}})\bar{\mathbf{u}} - \mathbf{s}_1^\mathrm{T}\mathbf{p} = \mathbf{f}_\mathrm{t}^\mathrm{e}. \tag{20}$$

It is important to note that deploying the nonlinear strain–displacement relationship is necessary to account for the effect of initial strain/stress on the stiffness of the system. In the subsequent analysis for small vibration, the nonlinear stiffness matrix, $\mathbf{k}_{\mathrm{t(NL)}}$, is neglected.

3.2. Fluid Domain

Upon applying a finite element method to the fluid equation, equation (14) can be reduced to a matrix equation in terms of coefficients representing the pressure matrix $\mathbf{p}$ at the nodal points of the finite-element mesh, respectively. The fluid domain is divided into finite-element sub-domains for the pressure field. The pressure field can be approximated in terms

of vectors of nodal pressures, viz.

$$p(x, \theta, r, t) = \mathbf{N}_f \mathbf{p}, \quad \delta p(x, \theta, r, t) = \delta \mathbf{p}^{\mathrm{T}} \mathbf{N}_{\mathrm{f}}^{\mathrm{T}}. \tag{21}$$

Applying a variational statement to equations (14)–(16), and neglecting nonlinear convection terms, the following equation is obtained:

$$\int_{\Omega_{\mathrm{f}}} \nabla p \cdot \nabla(\delta p)\, \mathrm{d}\Omega_{\mathrm{f}} - (1/a_{\mathrm{f}}^2) \int_{\Omega_{\mathrm{f}}} \ddot{p}\, \delta p\, \mathrm{d}\Omega_{\mathrm{f}} - \rho_{\mathrm{f}} \int_{\Gamma_{\mathrm{f}} \cap \Gamma_{\mathrm{t}}} [\mathbf{n} \cdot (\ddot{\mathbf{u}} + 2U\dot{\mathbf{u}}_{,s} + U^2 \mathbf{u}_{,ss})] \cdot \delta p \mathbf{n}\, \mathrm{d}\Gamma_{\mathrm{f}} = 0. \tag{22}$$

Upon substituting equations (17) and (21) into equation (22), the following equation for one element in the global coordinate system can be obtained:

$$\mathbf{ap} + \mathbf{e}\ddot{\mathbf{p}} - \mathbf{s}_1 \ddot{\bar{\mathbf{u}}} - \mathbf{s}_2 \dot{\bar{\mathbf{u}}} - \mathbf{s}_3 \bar{\mathbf{u}} = \mathbf{0}, \tag{23}$$

where

$$\mathbf{a} = (1/\rho_f) \int_{\Omega_{\mathrm{f}}} (\nabla \mathbf{N}_{\mathrm{f}})^{\mathrm{T}} \nabla \mathbf{N}_{\mathrm{f}}\, \mathrm{d}\Omega_{\mathrm{f}}, \ \mathbf{e} = (1/a_{\mathrm{f}}^2) \int_{\Omega_{\mathrm{f}}} \mathbf{N}_{\mathrm{f}}^{\mathrm{T}} \cdot \mathbf{N}_{\mathrm{f}}\, \mathrm{d}\Omega_{\mathrm{f}}, \ \mathbf{s}_1 = \int_{\Gamma_{\mathrm{f}} \cap \Gamma_{\mathrm{t}}} \mathbf{N}_{\mathrm{f}}^{\mathrm{T}} \cdot \mathbf{n} \cdot \mathbf{N}_{\mathrm{t}}\, \mathrm{d}\Gamma_{\mathrm{f}}, \tag{24a}$$

$$\mathbf{s}_2 = 2U \int_{\Gamma_{\mathrm{f}} \cap \Gamma_{\mathrm{t}}} \mathbf{N}_{\mathrm{f}}'^{\mathrm{T}} \cdot \mathbf{n} \cdot \mathbf{N}_{\mathrm{t}}\, \mathrm{d}\Gamma_{\mathrm{f}}, \ \mathbf{s}_3 = U^2 \textstyle\int_{\Gamma_{\mathrm{f}} \cap \Gamma_{\mathrm{t}}} \mathbf{N}_{\mathrm{f}}^{\mathrm{T}} \cdot \mathbf{n} \cdot \mathbf{N}_{\mathrm{t}}''\, \mathrm{d}\Gamma_{\mathrm{f}}. \tag{24b}$$

3.3. Coupling Equation

Upon assembling shell elemental matrices, the following equation governing the motion of the shell can be obtained:

$$\begin{bmatrix} \mathbf{M}_{\mathrm{tt}} & \mathbf{M}_{\mathrm{tb}} \\ \mathbf{M}_{\mathrm{bt}} & \mathbf{M}_{\mathrm{bb}} \end{bmatrix} \begin{Bmatrix} \ddot{\mathbf{U}}_{\mathrm{t}} \\ \ddot{\mathbf{U}}_{\mathrm{b}} \end{Bmatrix} + \begin{bmatrix} \mathbf{K}_{\mathrm{tt}} & \mathbf{K}_{\mathrm{tb}} \\ \mathbf{K}_{\mathrm{bt}} & \mathbf{K}_{\mathrm{bb}} \end{bmatrix} \begin{Bmatrix} \mathbf{U}_{\mathrm{t}} \\ \mathbf{U}_{\mathrm{b}} \end{Bmatrix} + \begin{bmatrix} \mathbf{0} & \mathbf{0} \\ \mathbf{0} & \mathbf{S}_1^{\mathrm{T}} \end{bmatrix} \begin{Bmatrix} \mathbf{0} \\ \mathbf{P}_{\mathrm{b}} \end{Bmatrix} = \begin{Bmatrix} \mathbf{F}_{\mathrm{t}} \\ \mathbf{F}_{\mathrm{b}} \end{Bmatrix}, \tag{25}$$

where $\{\mathbf{U}_{\mathrm{t}}^{\mathrm{T}}, \mathbf{U}_{\mathrm{b}}^{\mathrm{T}}\}^{\mathrm{T}}$ and $\{\ddot{\mathbf{U}}_{\mathrm{t}}^{\mathrm{T}}, \ddot{\mathbf{U}}_{\mathrm{b}}^{\mathrm{T}}\}^{\mathrm{T}}$ are the global displacement and acceleration vectors, respectively; and

$$\begin{bmatrix} \mathbf{M}_{\mathrm{tt}} & \mathbf{M}_{\mathrm{tb}} \\ \mathbf{M}_{\mathrm{bt}} & \mathbf{M}_{\mathrm{bb}} \end{bmatrix} \text{ and } \begin{bmatrix} \mathbf{K}_{\mathrm{tt}} & \mathbf{K}_{\mathrm{tb}} \\ \mathbf{K}_{\mathrm{bt}} & \mathbf{K}_{\mathrm{bb}} \end{bmatrix}$$

are the shell global mass and stiffness matrices, respectively.

Similarly, assembling fluid elemental matrices in the global coordinate system, we can obtain the equation governing the motion of the fluid:

$$\begin{bmatrix} \mathbf{A}_{\mathrm{ff}} & \mathbf{A}_{\mathrm{fb}} \\ \mathbf{A}_{\mathrm{bf}} & \mathbf{A}_{\mathrm{bb}} \end{bmatrix} \begin{Bmatrix} \mathbf{P}_{\mathrm{f}} \\ \mathbf{P}_{\mathrm{b}} \end{Bmatrix} + \begin{bmatrix} \mathbf{E}_{\mathrm{ff}} & \mathbf{E}_{\mathrm{fb}} \\ \mathbf{E}_{\mathrm{bf}} & \mathbf{E}_{\mathrm{bb}} \end{bmatrix} \begin{Bmatrix} \ddot{\mathbf{P}}_{\mathrm{f}} \\ \ddot{\mathbf{P}}_{\mathrm{b}} \end{Bmatrix} + \begin{bmatrix} \mathbf{0} & \mathbf{0} \\ \mathbf{0} & \mathbf{S}_1 \end{bmatrix} \begin{Bmatrix} \mathbf{0} \\ \ddot{\mathbf{U}}_{\mathrm{b}} \end{Bmatrix} + \begin{bmatrix} \mathbf{0} & \mathbf{0} \\ \mathbf{0} & \mathbf{S}_2 \end{bmatrix} \begin{Bmatrix} \mathbf{0} \\ \dot{\mathbf{U}}_{\mathrm{b}} \end{Bmatrix} + \begin{bmatrix} \mathbf{0} & \mathbf{0} \\ \mathbf{0} & \mathbf{S}_3 \end{bmatrix} \begin{Bmatrix} \mathbf{0} \\ \mathbf{U}_{\mathrm{b}} \end{Bmatrix} = \begin{Bmatrix} \mathbf{0} \\ \mathbf{0} \end{Bmatrix}, \tag{26}$$

where $\{\mathbf{P}_{\mathrm{t}}^{\mathrm{T}}, \mathbf{P}_{\mathrm{b}}^{\mathrm{T}}\}^{\mathrm{T}}$ is the global nodal pressure vector;

$$\begin{bmatrix} \mathbf{A}_{\mathrm{ff}} & \mathbf{A}_{\mathrm{fb}} \\ \mathbf{A}_{\mathrm{bf}} & \mathbf{A}_{\mathrm{bb}} \end{bmatrix} \text{ and } \begin{bmatrix} \mathbf{E}_{\mathrm{ff}} & \mathbf{E}_{\mathrm{fb}} \\ \mathbf{E}_{\mathrm{bf}} & \mathbf{E}_{\mathrm{bb}} \end{bmatrix}$$

are integral coefficient matrices of fluid pressures and the second-order derivative of fluid pressures with respect to time, respectively.

If the external force terms can be expressed as $\mathbf{F} = \{\mathbf{F}_t^T, \mathbf{F}_b^T\}^T = \mathbf{F}_0 e^{\omega_{mn}t}$, the solution will exist in the same form, i.e.

$$\mathbf{U} = \{\mathbf{U}_t^T, \mathbf{U}_b^T\}^T = \mathbf{U}_0 e^{\omega_{mn}t} \text{ and } \mathbf{P} = \{\mathbf{P}_t^T, \mathbf{P}_b^T\}^T = \mathbf{P}_0 e^{\omega_{mn}t}. \tag{27}$$

Substituting equation (27) into (26) and setting

$$\begin{bmatrix} \mathbf{A}_{ff} + \omega_{mn}^2 \mathbf{E}_{ff} & \mathbf{A}_{fb} + \omega_{mn}^2 \mathbf{E}_{fb} \\ \mathbf{A}_{bf} + \omega_{mn}^2 \mathbf{E}_{bf} & \mathbf{A}_{bb} + \omega_{mn}^2 \mathbf{E}_{bb} \end{bmatrix}^{-1} = \begin{bmatrix} \mathbf{H}_{ff}^{-1} & \mathbf{H}_{fb}^{-1} \\ \mathbf{H}_{bf}^{-1} & \mathbf{H}_{bb}^{-1} \end{bmatrix},$$

the following equation is obtained:

$$\mathbf{P}_b = \mathbf{H}_{bb}^{-1}\mathbf{S}_1\ddot{\mathbf{U}}_b + \mathbf{H}_{bb}^{-1}\mathbf{S}_2\dot{\mathbf{U}}_b - \mathbf{H}_{bb}^{-1}\mathbf{S}_3\mathbf{U}_b = \mathbf{H}_{bb}^{-1}(\omega_{mn}^2\mathbf{S}_1 + \omega_{mn}\mathbf{S}_2 + \mathbf{S}_3)\mathbf{U}_b, \tag{28}$$

where $\mathbf{H}_{bb}^{-1}$ is a frequency-dependent matrix.

Substituting equation (28) into equation (25) leads to

$$\left(\omega_{mn}^2 \begin{bmatrix} \mathbf{M}_{tt} & \mathbf{M}_{tb} \\ \mathbf{M}_{bt} & \mathbf{M}_{bb} + \mathbf{M}_f \end{bmatrix} + \omega_{mn} \begin{bmatrix} \mathbf{0} & \mathbf{0} \\ \mathbf{0} & \mathbf{C}_f \end{bmatrix} + \begin{bmatrix} \mathbf{K}_{tt} & \mathbf{K}_{tb} \\ \mathbf{K}_{bt} & \mathbf{K}_{bb} + \mathbf{K}_f \end{bmatrix}\right) \begin{Bmatrix} \mathbf{U}_t \\ \mathbf{U}_b \end{Bmatrix} = \begin{Bmatrix} \mathbf{F}_t \\ \mathbf{F}_b \end{Bmatrix}, \tag{29}$$

where $\mathbf{M}_f$, $\mathbf{C}_f$ and $\mathbf{K}_f$ are the frequency-dependent hydrodynamic mass, damping and stiffness matrices associated with the inertia, Coriolis and centrifugal forces, respectively. For the case of incompressibility, these mass, damping and stiffness matrices are frequency independent.

4. RESULTS AND DISCUSSION

To the authors' knowledge, there are no published experimental results on the vibration of orthotropic shells. Our new model has therefore been compared with the results of previous and established analyses to assess its validity, and only after this verification was it finally applied to orthotropic shells conveying fluid. We have explored the effects of flowing fluid and different orthotropic material properties on the vibration of the system, and have been able to demonstrate the usefulness of our approach to this modelling.

In all subsequent calculation examples, the three principal directions of elasticity coincide with the directions of the axes. A convergence study has been conducted for isotropic cylindrical shells conveying fluid by Zhang *et al.* (2001). For isotropic thin cylindrical shells conveying fluid at a circumferential wavenumber $n = 2$ and longitudinal half-wavenumber $m = 3$, natural frequencies converge to less than 0·2% error for a system which is discretized into 20×1 finite elements (axial × radial) for the shell domain and 20×4 finite elements for the fluid domain, respectively. A similar convergence analysis has also been conducted for initially tensioned orthotropic cylindrical shells conveying fluid, but not presented here for reasons of conciseness. For orthotropic cylindrical shells conveying fluid with a thickness–radius ratio $h/R = 0{\cdot}3$, frequencies can stabilize with a relative error less than 0·2% for a system which is discretized into 20×3 for the shell domain and 20×4 for the fluid domain.

We first considered transversely isotropic cylindrical shells in the absence of and containing fluid. The free vibration of this system was analysed using the material properties outlined in Table 1, which were also used by Jain (1974) and Chen & Ding (1999). When considering the fluid-filled system, the following physical data are used to capture and exemplify significant features: $\rho_t = 7130\ \text{kg/m}^3$, $\rho_f/\rho_t = 0{\cdot}091$ and $a_f/a_t = 0{\cdot}3$. These shells are simply supported at both ends. Two cases, (i) the shells in the absence of and (ii) containing compressible fluid, were analysed for vibration modes with a circumferential wavenumber $n = 2$ and axial half-wavenumber $m = 1$.

TABLE 1
Material properties of the zinc cylindrical shells

Material	Elastic constants ($N\,m^{-2}$)	
Transversely isotropic (Zinc)	$D_{22} = D_{33} = 1{\cdot}5825 \times 10^{11}$ $D_{12} = D_{13} = 0{\cdot}4744 \times 10^{11}$ $D_{44} = D_{66} = 0{\cdot}40 \times 10^{11}$	$D_{11} = 0{\cdot}6160 \times 10^{11}$ $D_{23} = 0{\cdot}3151 \times 10^{11}$ $D_{55} = 0{\cdot}6337 \times 10^{11}$

TABLE 2
Comparison of the lowest dimensionless natural frequencies obtained from the present model with existing theoretical results for a simply-supported fluid-filled zinc cylindrical shell at $mR/L = 0{\cdot}4$ and $n = 2$

		Dimensionless natural frequencies $\bar{\omega}_{mn} = \omega_{mn} R(\rho_t/D_{66})^{1/2}$				
$(\bar{a}, \bar{\rho})$	h/R	Classical shell theory (Dong 1968)	Analytical model (Chen & Ding 1999)	Five-mode shell theory (Jain 1974)	Six-mode shell theory (Mirsky 1964)	Present FE model
(0, 0)	0·01	0·302159	0·301727	0·301748	0·301773	0·30285
	0·05	0·326250	0·316059	0·316552	0·31743	0·32041
	0·10	0·391960	0·356556	0·358234	0·35915	0·35915
(0·2, 0·1)	0·01	0·152701	0·143356	0·152733	0·143191	0·14451
	0·05	0·256069	0·241767	0·249875	0·241706	0·24834
	0·10	0·338637	0·305744	0·312881	0·307336	0·31217
(0·3, 0·1)	0·01	0·153812	0.144480	0·153834	0·144312	0·14511
	0·05	0·258922	0·244716	0·252351	0·244683	0.24984
	0·10	0·343301	0·309565	0·315929	0·311333	0·31935
(0·2, 0·3)	0·01	0·097676	0·090686	0·097720	0·090559	0·09056
	0·05	0·195370	0·181591	0·191098	0·181150	0·18509
	0·10	0·280389	0·250970	0·260604	0·251222	0·25572
(0·5, 0·4)	0·01	0·079785	0·079901	0·086242	0·079875	0·07932
	0·05	0·166670	0·167164	0·176399	0·166670	0·16741
	0·10	0·238486	0·238442	0·247810	0·238486	0·23696

The comparison of the predicted results obtained by our model and those obtained from the five-mode shell theory (Jain 1974), the analytical model (Chen & Ding 1999), the classical shell theory (Dong 1968) and the six-mode shell theory (Mirsky 1964), is presented in Table 2. It can be seen from the table that there is a good agreement between our theory and the other results obtained using the five- and six-mode theories and the analytical model of Chen & Ding. This demonstrates the validity of the present model for the cases of transversely isotropic cylindrical shells in the absence of, and containing, fluid.

It can be seen that for the thin shells containing compressible fluid, the frequencies obtained using the present model are closer to those obtained using the six-mode shell theory than the five-mode shell theory. This is due to the neglect of transverse normal strain in the five-mode shell theory. It also can be seen that for a moderately thick shell (i.e., $h/R > 0{\cdot}05$), there is a large relative error in frequencies obtained using the classical shell theory and the other four shell theories. Hence, the classical shell theory is not applicable to even slightly thick shells containing fluid. As expected, natural frequencies decrease as fluid

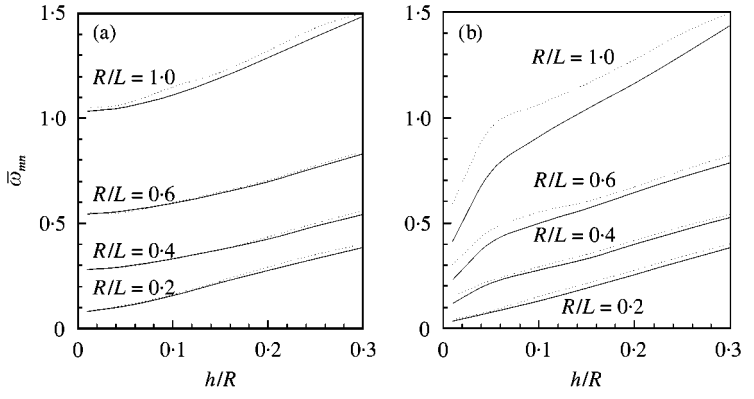

Figure 2. Transversely isotropic shell: variation of natural frequencies with thickness-to-radius and radius-to-length ratios at circumferential wavenumber $n = 2$: - - - - -, theoretical results (Jain 1974); ——, present model. (a) Empty shell; (b) fluid-filled shell.

densities increase. For $\bar{\rho} = \rho_f/\rho_t = 0{\cdot}1$, natural frequencies increase by 1·0–1·5% when the fluid compressibility decreases by 55·5%.

For the shell in the absence of and containing incompressible fluid (water), the dimensionless natural frequencies $\bar{\omega}_{mn} = \omega_{mn}R\{\rho_t/(D_{11} - D_{13}^2/D_{33})\}^{1/2}$ are shown in Figure 2. It can be seen that natural frequencies obtained using the present FE model generally agree well with the theoretical results obtained by using the five-mode shell theory (Jain 1974). But for the case of fluid-filled shells with $R/L = 1{\cdot}0$, the difference in frequency obtained using the present model and the five-mode shell theory reaches around 20%. This is probably due to too few mode terms being used in the application of the Rayleigh–Ritz method for the coupled dynamic problem of short cylindrical shells. However, as expected, frequencies increase as thickness-to-radius and radius-to-length ratios increase. It can also be seen that the presence of fluid lowers the frequencies more significantly for thin shells than for thick shells.

The effect of initial compression forces on the natural frequencies of an empty orthotropic cylindrical shell has also been analysed. The following material properties, in the shell material principal axes, were considered: $E_1 = 1727$ GPa, $E_2 = 7{\cdot}2$ GPa, $\nu_{12} = 0{\cdot}26$, $G_{12} = G_{13} = G_{23} = 3{\cdot}76$ GPa, $\rho_t = 1550$ kg/m^3, $R/h = 25$, $L/R = 4$. For such thin shells, it is assumed that σ_{rr} is equal to zero. Figure 3 shows the comparison of dimensionless natural frequencies, $\bar{\omega}_{mn} = \omega_{mn}L(\rho_t/E_2)^{1/2}$, obtained using the present model with the theoretical results of Sivadas (1995) under various dimensionless axial compression forces, $\bar{T} = T_x(1 - \nu_{12}^2)/E_2Rh$. It can be seen from this figure that frequencies decrease as compression forces increase, as expected, and the results of our model agree well with the theory of Sivadas (1995).

In the next set of calculations, the following dimensionless flow velocities, $\bar{U} = v_0/v_a$ and natural frequencies, $\bar{\omega}_{mn} = \omega_{mn}/\omega_a$ were adopted, where v_a and ω_a are given by $v_a = [E/\rho_s(1 - \nu^2)]^{1/2}$ and $\omega_a = (1/R)\{E/\rho_s(1 - \nu^2)\}^{1/2}$. The effect of internal fluid flow on the dynamic behaviour of thin cylindrical shells was investigated, with physical properties corresponding to those of a latex rubber cylindrical shell conveying air, which has been tested experimentally by Païdoussis & Denise (1972). The physical properties are: $\rho_t = 850$ kg m^{-3}, $E = 8{\cdot}957 \times 10^5$ Nm^{-2}, $\nu = 0{\cdot}5$, $\rho_f/\rho_t = 0{\cdot}00136$, $R/h = 44{\cdot}1$ and $L/R = 3{\cdot}225 - 32{\cdot}35$.

Dimensionless critical flow velocities, $\bar{U}$, for the onset of flutter of the cylindrical shell clamped at one end and free at the other end were calculated and compared with

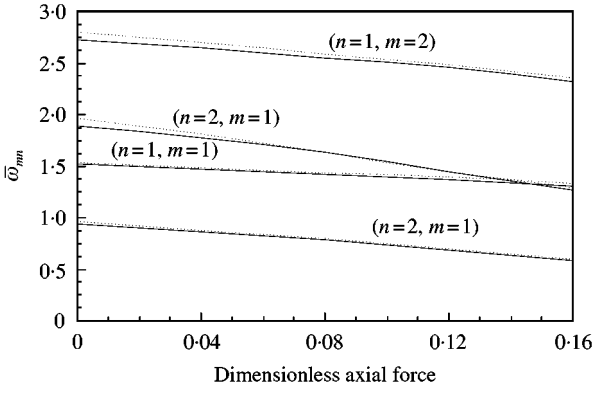

Figure 3. Empty orthotropic shell: comparison of dimensionless natural frequencies obtained from present model with theoretical results: ——, present model; - - - - -, theory (Sivadas 1995).

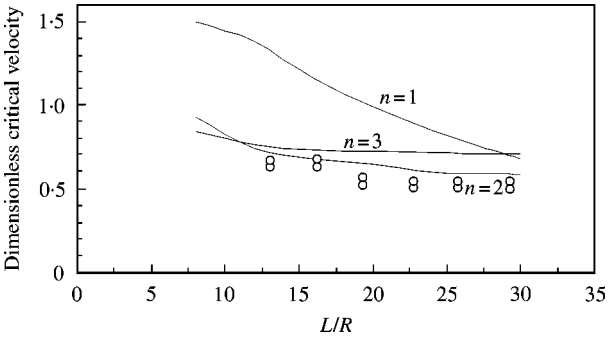

Figure 4. Comparison of present numerical results with experimental results for cylindrical shells with clamped–clamped boundary conditions: ○, experiment (Païdoussis & Denise 1972); ——, present model.

experimental results (Païdoussis & Denise 1972), as shown in Figure 4. It can be seen from this figure that critical flow velocities obtained by using the present method generally agree reasonably with experiment, although for $L/R < 15$ the difference between experiment and theory is quite large. This is also reflected in the comparison of Païdoussis & Denise's analytical and experimental results.

Given this good agreement with previous results, the next calculation examined the effect of fluid flow velocities on the free vibration of zinc cylindrical shells conveying water. The material properties from the first example were again used. Figures 5 and 6 show the variation of dimensionless natural frequencies, $\bar{\omega}_{mn} = \omega_{mn} R\{\rho_t/(D_{11} - D_{13}^2/D_{33})\}^{1/2}$, with dimensionless flow velocities $\bar{U} = U(\rho_t/D_{66})^{1/2}$, for a circumferential wavenumber $n = 2$ and longitudinal half-wavenumber $m = 1, 2$. It can be seen that natural frequencies decrease with increasing flow velocity, as expected. It also can be seen from these figures that dimensionless critical velocities increase as thickness-to-radius and radius-to-length ratios increase. Natural frequencies also increase with increasing initial axial tension.

The final calculation analysed the effect of material properties on the natural frequency of the system. We considered a fluid-conveying initially-tensioned orthotropic cylindrical shell simply supported at both ends with the following physical data: $D_{11}/D_{66} = 10, 3{\cdot}75, 1{\cdot}5,$

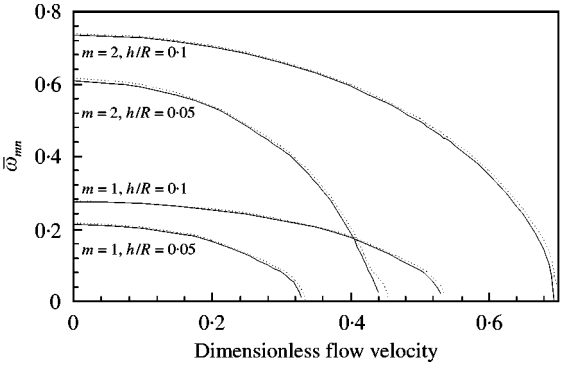

Figure 5. Transversely isotropic shell conveying water: effect of thickness-to-radius ratio on the dimensionless natural frequency at $R/L = 0{\cdot}4$ and $n = 2$: ——, $\bar{T} = 0$; ------, $\bar{T} = 0{\cdot}06$.

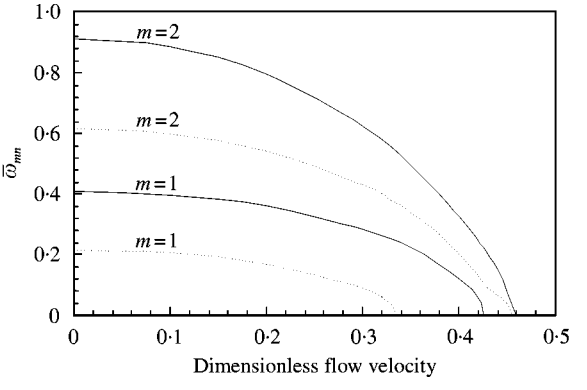

Figure 6. Transversely isotropic shell conveying water: effect of thickness-to-radius ratio on the dimensionless natural frequency at $\bar{T} = 0{\cdot}06$ and $n = 2$: ——, $R/L = 0{\cdot}6$; -----, $R/L = 0{\cdot}4$.

$D_{22} = 4{\cdot}0D_{66}$, $D_{12} = 1{\cdot}25D_{66}$, $D_{13} = 1{\cdot}0D_{66}$, $D_{23} = 0{\cdot}75D_{66}$, $D_{33} = 3{\cdot}75D_{66}$, $D_{44} = 1{\cdot}75D_{66}$, $D_{55} = 1{\cdot}75D_{66}$, $\rho_f/\rho_t = 0{\cdot}14$, $R/L = 0{\cdot}4$, $R/h = 20$. Figure 7 shows the variation of dimensionless natural frequency with fluid-flow velocity for the three values of D_{11}/D_{66}, for a circumferential wavenumber $n = 2$ and longitudinal half-wavenumber $m = 1, 2$. It can be seen that the bigger the value of D_{11}/D_{66} (which corresponds to the axial stiffness) the larger the critical flow velocity. All the curves display the previous trend of natural frequencies decreasing with increasing fluid-flow velocities. Figure 8 shows the variation of dimensionless natural frequency for the first three longitudinal half-wavenumbers with the circumferential wavenumber (which is taken as a continuous variable). It can be seen that the minimum natural frequency occurs at $n = 3$ and $m = 1$ regardless of the value of D_{11}/D_{66} It may be noted that for $D_{11}/D_{66} = 1{\cdot}5$, the natural frequency at vibration mode $m = 3$ and $n = 1$ is smaller than that at vibration mode $m = 3$ and $n = 2$. This is due to the low axial stiffness.

5. CONCLUSIONS

A finite-element formulation for the vibration of initially tensioned orthotropic cylindrical shells conveying compressible inviscid fluid has been presented. A nonlinear

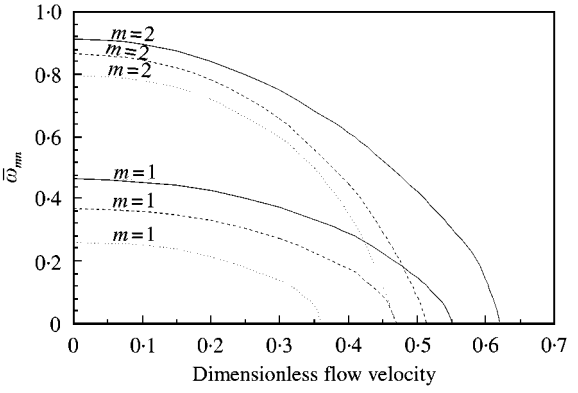

Figure 7. Orthotropic shell conveying fluid: variation of dimensionless natural frequency with fluid flow velocity at dimensionless initial axial tension $\bar{T} = 0{\cdot}06$ and circumferential wavenumber $n = 2$: ——, $D_{11}/D_{66} = 10$; — —, $D_{11}/D_{66} = 3{\cdot}75$; - - - - -, $D_{11}/D_{66} = 1{\cdot}5$.

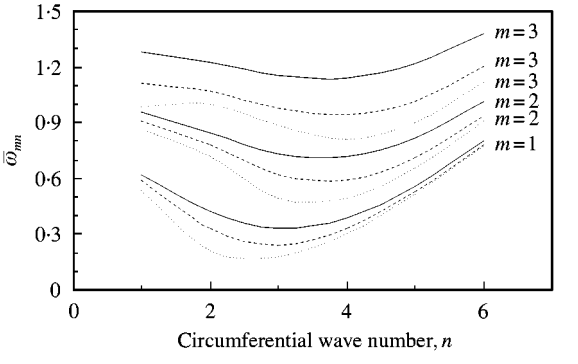

Figure 8. Orthotropic shell conveying fluid: variation of dimensionless natural frequency with circumferential wavenumber at dimensionless initial axial tension $\bar{T} = 0{\cdot}06$ and fluid flow velocity $\bar{U} = 0{\cdot}2$: ——, $D_{11}/D_{66} = 10$; — —, $D_{11}/D_{66} = 3{\cdot}75$; - - - - - -, $D_{11}/D_{66} = 1{\cdot}5$.

strain–displacement relationship was employed to derive the geometric stiffness matrix due to initial stresses and hydrostatic pressures. Frequency-dependent fluid mass, damping and stiffness matrices associated with inertia, Coriolis and centrifugal forces, respectively, were derived given the fluid–structure coupling condition. The method is based on the three-dimensional theory of elasticity and Euler's equation. Numerical examples were given to demonstrate that the present model can be readily applied to the coupled dynamic problem of initially tensioned orthotropic thin or thick cylindrical shells conveying fluid with reasonable accuracy.

It was shown that natural frequencies increase as thickness-to-radius and radius-to-length ratios and initial axial tensions increase, or fluid flow velocities and fluid densities decrease, as expected. It was also shown that natural frequencies increase slightly as fluid compressibility decreases. The effect of fluid compressibility on natural frequency can, however, be neglected for a larger fluid density, for example $\bar{\rho} = 0{\cdot}1$. For orthotropic shells conveying fluid, the larger the axial stiffness, the larger the critical flow velocity. Minimum natural frequency occurs at a certain vibration mode, regardless of the axial stiffness for all the cases examined. It is interesting to note that when the minimum natural frequency

occurs at the third circumferential wavenumber ($n = 3$), natural frequencies at $n = 1$ may be smaller than that at $n = 2$ for low axial stiffness.

The model developed here is capable of handling the influence of variation in thin/thick shell geometrical and material parameters, and the effect of fluid flow velocities, hydrostatic pressures and initial tension/compression on the dynamic behaviour. In the course of establishing the model, nonlinear shell stiffness terms and flow convection terms were neglected. Also, the lateral fluid pressure is assumed to be constant directional, and perturbations originating from the shell oscillation at both inlet and outlet of the shell were assumed to be negligible. These are limitations in this vibratory analysis, as it stands. Future effort will be directed to incorporating variable lateral pressure, in terms of direction and magnitude per unit area, fluid convection terms and nonlinear stiffness terms, and examining the effect of nonlinearity on the vibration.

References

Bittnar, Z. & Sejnoha, J. 1996 *Numerical methods in structural mechanics*. London: Thomas Telford Publications.

Bradford, L. G. & Dong, S. B. 1978 Lateral vibrations of orthotropic cylinders under initial stress. *Journal of Sound and Vibration* **60**, 157–175.

Chang, J. S. & Chiou, W. J. 1995 Natural frequencies and critical velocities of fixed-fixed laminated circular cylindrical shells conveying fluids. *Computers and Structures* **57**, 929–939.

Chebair, A. El, Païdoussis, M. P. & Mirsa, A. K. 1989 Experimental study of annular-flow-induced instabilities of cylindrical shells. *Journal of Fluids and Structures* **3**, 349–364.

Chen, S. S. 1987 *Flow-induced Vibration of Circular Structures*. Washington: Hemisphere Publishing Corporation.

Chen, W. Q. & Ding, H. J. 1999 Natural frequencies of fluid-filled transversely isotropic cylindrical shells. *International Journal of Mechanical Sciences* **41**, 677–684.

Chen, W. Q., Ding, H. J., Guo, Y. H. & Yang, Q. D. 1997 Free vibrations of fluid-filled orthotropic cylindrical shells. *Journal of Engineering Mechanics* **123**, 1130–1133.

Dong, S. B. 1968 Free vibration of laminated orthotropic cylindrical shells. *Journal of the Acoustical Society of America* **44**, 1628.

Jain, R. K. 1974 Vibration of fluid-filled, orthotropic cylindrical shells. *Journal of Sound and Vibration* **37**, 379–388.

Lakis, A. A. & Selmane, A. 1997 Vibration analysis of anisotropic open cylindrical shells subjected to a flowing fluid. *Journal of Fluids and Structures* **11**, 111–134.

Lekhnitskii, S. G. 1963 *Theory of Elasticity of an Anisotropic Elastic Body*. San Francisco: Holden-Day Inc.

Mirsky, I. 1964 Vibrations of orthotropic, thick, cylindrical shells. *Journal of the Acoustical Society of America* **36**, 41–51.

Païdoussis, M. P. & Denise, J.-P. 1972 Flutter of thin cylindrical shells conveying fluid, *Journal of Sound and Vibration* **20**, 9–26.

Païdoussis, M. P & Mateescu, A. D. 1987 Dynamics of cylindrical shell containing fluid flows with a developing boundary layer. *AIAA Journal* **25**, 1985, 857–863.

Païdoussis, M. P., Mirsa, A. K. & Chan, S. P. 1985 Dynamics and stability of coaxial cylindrical shells conveying viscous fluid, *Journal of Applied Mechanics* **52**, 389–396.

Ramasamy, R. & Ganesan, N. 1999 Vibration and damping analysis of fluid filled orthotropic cylindrical shells with constrained viscoelastic damping. *Computers and Structures* **70**, 363–376.

Shang, S. P. & Lei, G. P. 1988 The free vibration of orthotropic moderately thick shells conveying fluid. In *Applications of Mechanics in Engineering*, Hangzhou, pp. 231–241.

Sharma, C. B., Darvizeh, M. & Darvizeh, A. 1996 Free vibration response of multilayered orthotropic fluid-filled circular cylindrical shells. *Composite Structures* **34**, 349–355.

Sharma, C. B., Darvizeh, M. & Darvizeh, A. 1998 Natural frequency response of vertical cantilever composite shells containing fluid. *Engineering Structures* **20**, 732–737.

Sivadas, K. R. 1995 Vibration analysis of pre-stressed thick circular conical composite shells. *Journal of Sound and Vibration* **186**, 87–97.

Weaver, D. S. & Unny, T. E. 1973 On the dynamic stability of fluid conveying pipes. *Journal of Applied Mechanics* **40**, 48–52.

ZHANG, Y. L., REESE, J. M. & GORMAN, D. G. 2001 A comparative study of axisymmetric finite elements for the vibration of thin cylindrical shells conveying fluid. *International Journal for Numerical Methods in Engineering* (submitted).

ZIENKIEWICZ, O. C. & TAYLOR, R. L. 1991 *The Finite Element Method*. Vol. 2, 4th ed. London: McGraw-Hill.

APPENDIX A. NOMENCLATURE

a_f, a_t	sound velocity in the fluid and elastic wave velocity of the shell, respectively, i.e. $a_t = (D_{44}/\rho_t)^{1/2}$, $a_f = (K/\rho_f)^{1/2}$
$\bar{a}$	$\bar{a} = a_f/a_t$
$\mathbf{a}$	integral coefficient matrix of fluid pressure, defined by equation (24a)
$\mathbf{A}_{bb}$	integral coefficient of the pressure over the fluid–strucutre interface
$\mathbf{A}_{fb}$	integral coefficient of the pressure over the fluid domain adjacent to the fluid–structure interface, i.e. $\mathbf{A}_{fb} = \mathbf{A}_{bf}^T$
$\mathbf{A}_{ff}$	integral coefficient of the pressure over the fluid domain excluding the fluid boundary domain adjacent to the fluid–structure interface
$\mathbf{B}_L$, $\mathbf{B}_{NL}$	linear and nonlinear strain–displacement matrices, respectively
$\mathbf{C}_f$	fluid damping matrix associated with the Coriolis force, i.e. $\mathbf{C}_f = \mathbf{S}_1^T\mathbf{H}_{bb}^{-1}\mathbf{S}_2$
d, D	internal and external diameters, respectively
D_{ij}	nine independent elastic constants, defined by equation (AII.1)
$\mathbf{D}$	shell stress–strain matrix defined by equations (4) and (5)
$\mathbf{e}$	integral coefficient matrix of the second-order derivative of fluid pressure, defined by equation (24a)
E	Young's modulus
E_1, E_2	Young's moduli in material principal axes, respectively
E_{xx}, $E_{\theta\theta}$, E_{rr}	Young's moduli in the axial, tangential and radial directions, respectively
$\mathbf{E}_{bb}$	integral coefficient of the second-order derivative of pressure with respect to time over the fluid–structure interface
$\mathbf{E}_{fb}$	integral coefficient of the second-order derivative of pressure with respect to time over the fluid domain adjacent to the fluid–structure interface, i.e. $\mathbf{E}_{fb} = \mathbf{E}_{bf}^T$
$\mathbf{E}_{ff}$	integral coefficient of the second-order derivative of pressure with respect to time over the fluid domain excluding the fluid boundary domain adjacent to the fluid–structure interface
$\mathbf{f}_t^e$	vector of the elemental nodal external forces exerted on the shell
$\{\mathbf{F}_t^T, \mathbf{F}_b^T\}$	vector of the global nodal external force exerted on the shell
G	shear modulus
G_{12}, G_{13}, G_{23}	shear moduli in material principal axes, respectively
$G_{x\theta}$, G_{rx}, $G_{\theta r}$	shear moduli which characterize the variation of the angles in the directions x and θ, r and x, and θ and r, respectively
$\mathbf{G}$	matrix defined by equation (AII.5)
h	shell thickness
$\mathbf{H}_1$, $\mathbf{H}_2$	matrices defined by equations (AII.2) and (AII.3)
$\mathbf{I}_3$	unit matrix of order 3
$\mathbf{k}_t$	elemental shell stiffness matrix, i.e. $\mathbf{k}_t = \mathbf{k}_{t(L)} + \mathbf{k}_{t(NL)}$
K	bulk modulus of the fluid
$\mathbf{K}_f$	fluid stiffness matrix associated with the centrifugal force, i.e. $\mathbf{K}_f = \mathbf{S}_1^T\mathbf{H}_{bb}^{-1}\mathbf{S}_3$.

L	shell length
m, n	mth longitudinal and nth circumferential vibration modes, respectively
$\mathbf{m}_t$	elemental shell mass matrix, respectively
$\mathbf{M}_f$	fluid mass matrix associated with the inertia force, i.e. $\mathbf{M}_f = \mathbf{S}_1^T \mathbf{H}_{bb}^{-1} \mathbf{S}_1$
$\mathbf{n}$	unit outward vector normal to the fluid-structure interface (from the shell into the fluid)
$\mathbf{N}_t$, $\mathbf{N}_f$	matrices of shape function for the shell and fluid, respectively
$\mathbf{N}_T$	matrix defined by equation (B.6)
p_0	hydrostatic pressure
p	fluid pressure
$\mathbf{p}$	vector of nodal fluid pressure
$\mathbf{p}_f$	stress tensor exerted on the fluid at the fluid–structural interfaces
$\mathbf{p}_t$, $\mathbf{q}_t$	vectors of the prescribed shell boundary traction arising from fluid–structure interface interaction and external forces, respectively;
$\mathbf{P}_b$	generalized global nodal radial traction vector due to fluid pressures
$\mathbf{P}_f$	generalized global nodal fluid pressure vector for fluid elements excluding fluid–structure boundary elements.
R	shell mean radius
$\mathbf{s}_1$, $\mathbf{s}_2$, $\mathbf{s}_3$	matrices defined by equation (24a,b)
$\mathbf{S}$	matrix defined by equation (B.6)
$\mathbf{S}_1$, $\mathbf{S}_2$, $\mathbf{S}_3$	integral matrices over the fluid–structure interface, respectively
t	time
$\mathbf{t}$	unit vector tangential to the pipe surface
T_x, $\bar{T}$	dimensional and dimensionless axial forces, respectively
u_x, u_θ, u_r	axial, tangential and radial displacements, respectively;
U	fluid scalar velocity
$\bar{U}$	dimensionless flow velocity
$\mathbf{u}$	dynamic displacement vector of the shell
$\bar{\mathbf{u}}$	nodal displacement vector, i.e., $\bar{\mathbf{u}} = \{\bar{u}_{xi}, \bar{u}_{\theta i}, \bar{u}_{ri}, \varphi_i, \bar{u}_{xj}, \bar{u}_{\theta j}, \bar{u}_{rj}, \varphi_j\}^T$
$\mathbf{U}$	global generalized displacement vector
$\mathbf{U}_b$, $\mathbf{U}_t$	vectors of the generalized radial global nodal displacements for the shell elements adjacent to the fluid domain and the generalized global nodal displacement vector excluding radial nodal displacement for shell elements adjacent to the fluid domain
$\mathbf{v}$	flow velocity vector, i.e. $\mathbf{v} = v_r\mathbf{i} + v_\theta\mathbf{j} + v_x\mathbf{k}$
$V(\mathbf{u})$	strain energy of the shell
$W(\mathbf{u})$	energy of external forces on the shell
β_i	defined by equation (AII.4), ($i = 1, 2, \ldots, 9$)
$\gamma_{x\theta}$, $\gamma_{\theta r}$, γ_{rx}	shear strain components in cylindrical coordinates
Γ_t, Γ_f	shell and fluid boundary, respectively
$\Gamma_t \cap \Gamma_f$	shell and fluid-sharing boundary
$\boldsymbol{\varepsilon}$, $\boldsymbol{\varepsilon}^0$	strain and initial strain vectors of the shell, respectively
ε_{xx}, $\varepsilon_{\theta\theta}$, ε_{rr}	strain components in cylindrical coordinates
v	Poisson ratio
$v_{\theta x}$, v_{xr}, $v_{r\theta}$	Poisson coefficients which characterize tensions (compressions) in the x-, r- and θ-direction for compressions (tensions) in the θ-, x- and r- directions, respectively
Π	total potential energy of the shell
ρ_t, ρ_f	densities of the shell and fluid, respectively

$\boldsymbol{\rho}_t$	shell inertia force–acceleration matrix
$\bar{\rho}$	$\bar{\rho} = \rho_f/\rho_t$
$\boldsymbol{\sigma}$, $\boldsymbol{\sigma}_0$	stress and initial stress vectors, respectively, i.e. $\boldsymbol{\sigma}_0 = \{\sigma^0_{xx}, \sigma^0_{\theta\theta}, \sigma^0_{rr}, \tau^0_{xx}, \tau^0_{\theta\theta}, \tau^0_{rr}\}^T$
σ_{xx}, $\sigma_{\theta\theta}$, σ_{rr}	stress components in cylindrical coordinates
$\tau_{x\theta}$, $\tau_{\theta r}$, τ_{rx}	shear stress components in cylindrical coordinates
ω_{mn}, $\bar{\omega}_{mn}$	dimensional and dimensionless frequencies, respectively
$\boldsymbol{\nabla}$	$\boldsymbol{\nabla} = (\partial/\partial r)\mathbf{i} + (\partial/r\partial\theta)\mathbf{j} + (\partial/\partial x)\mathbf{k}$
Ω_t, Ω_f	shell and fluid spatial domains, respectively

Subscripts

L, NL	linear and nonlinear components, respectively
m, n	mth longitudinal and nth circumferential vibration modes, respectively
t, f	shell and fluid quantities, respectively

Superscript

T	transpose of matrix

APPENDIX B. LIST OF MATRICES

For an orthotropic material, components, D_{ij}, are given by

$$D_{11} = E_{xx}(1 - \nu_{\theta r}\nu_{r\theta})/\Xi;\ D_{22} = E_{\theta\theta}(1 - \nu_{xr}\nu_{rx})/\Xi;\ D_{33} = E_{rr}(1 - \nu_{x\theta}\nu_{\theta x})/\Xi;$$
$$D_{44} = G_{x\theta};\ D_{55} = G_{\theta r};\ D_{66} = G_{xr};\ D_{12} = E_{xx}(\nu_{\theta x} + \nu_{rx}\nu_{\theta r})/\Xi;$$
$$D_{13} = E_{xx}(\nu_{rx} + \nu_{rx}\nu_{\theta x})/\Xi;\ D_{23} = E_{xx}(\nu_{r\theta} + \nu_{rx}\nu_{x\theta})/\Xi;$$
$$\text{and } \Xi = 1 - \nu_{x\theta}\nu_{\theta x} - \nu_{r\theta}\nu_{\theta r} - \nu_{rx}\nu_{xr} - 2\nu_{\theta x}\nu_{xr}\nu_{r\theta}. \tag{B.1}$$

For a transversely isotropic material whose behaviour is independent of direction in the plane $x = 0$, $D_{22} = D_{33}$, $D_{12} = D_{13}$, $D_{44} = D_{66}$, and $D_{55} = \frac{1}{2}(D_{33} - D_{23})$.

The matrices, $\mathbf{H}_1$ and $\mathbf{H}_2$, are given by

$$\mathbf{H}_1 = \begin{bmatrix} 1 & 0 & 0 & 0 & 0 & 0 & 0 & 0 & 0 \\ 0 & 1 & 0 & 0 & 0 & 0 & 0 & 0 & 0 \\ 0 & 0 & 1 & 0 & 0 & 0 & 0 & 0 & 0 \\ 0 & 0 & 0 & 1 & 1 & 0 & 0 & 0 & 0 \\ 0 & 0 & 0 & 0 & 0 & 1 & 1 & 0 & 0 \\ 0 & 0 & 0 & 0 & 0 & 0 & 0 & 1 & 1 \end{bmatrix}, \tag{B.2}$$

$$\mathbf{H}_2 = \begin{bmatrix} \beta_1 & 0 & 0 & 0 & \beta_5 & 0 & 0 & \beta_8 & 0 \\ 0 & \beta_2 & 0 & \beta_4 & 0 & \beta_6 & 0 & 0 & 0 \\ 0 & 0 & \beta_3 & 0 & 0 & 0 & \beta_7 & 0 & \beta_9 \\ 0 & \beta_5 & 0 & \beta_1 & 0 & \beta_8 & 0 & 0 & 0 \\ 0 & \beta_7 & 0 & \beta_9 & 0 & \beta_3 & 0 & 0 & 0 \\ 0 & 0 & \beta_8 & 0 & 0 & 0 & \beta_5 & 0 & \beta_1 \end{bmatrix}. \tag{B.3}$$

The components β_i $(i = 1, \ldots, 9)$ in the matrix $\boldsymbol{\beta}$ are

$$\beta_1 = u_{x,x},\ \beta_2 = (u_{\theta,\theta} + u_r)/r,\ \beta_3 = u_{r,r},\ \beta_4 = u_{x,\theta}/r,\ \beta_5 = u_{\theta,x},$$
$$\beta_6 = (u_{r,\theta} - u_\theta)/r,\ \beta_7 = u_{\theta,r},\ \beta_8 = u_{r,x},\ \beta_9 = u_{x,r}. \tag{B.4}$$

The matrices $\mathbf{G}$, $\mathbf{N}_\mathrm{T}$ and $\mathbf{S}$ are given respectively by

$$\mathbf{G} = \begin{bmatrix} \mathbf{N}_{\mathrm{t},x}^\mathrm{T} & \mathbf{0} & \mathbf{0} & \mathbf{N}_{\mathrm{t},\theta}^\mathrm{T}/r & \mathbf{0} & \mathbf{0} & \mathbf{N}_{\mathrm{t},r}^\mathrm{T} & \mathbf{0} & \mathbf{0} \\ \mathbf{0} & \mathbf{N}_{\mathrm{t},x}^\mathrm{T} & \mathbf{0} & \mathbf{0} & \mathbf{N}_{\mathrm{t},\theta}^\mathrm{T}/r & -\mathbf{N}_\mathrm{t}^\mathrm{T}/r & \mathbf{0} & \mathbf{N}_{\mathrm{t},r}^\mathrm{T} & \mathbf{0} \\ \mathbf{0} & \mathbf{0} & \mathbf{N}_{\mathrm{t},x}^\mathrm{T} & \mathbf{0} & \mathbf{N}_\mathrm{t}^\mathrm{T}/r & \mathbf{N}_{\mathrm{t},\theta}^\mathrm{T}/r & \mathbf{0} & \mathbf{0} & \mathbf{N}_{\mathrm{t},r}^\mathrm{T} \end{bmatrix}^\mathrm{T}. \tag{B.5}$$

$$\mathbf{N}_\mathrm{T} = \begin{bmatrix} \mathbf{N}_\mathrm{t} & \mathbf{0} & \mathbf{0} \\ \mathbf{0} & \mathbf{N}_\mathrm{t} & \mathbf{0} \\ \mathbf{0} & \mathbf{0} & \mathbf{N}_\mathrm{t} \end{bmatrix}, \quad \mathbf{S} = \begin{bmatrix} \sigma_{xx}^0\mathbf{I}_3 & \tau_{x\theta}^0\mathbf{I}_3 & \tau_{xr}^0\mathbf{I}_3 \\ \tau_{x\theta}^0\mathbf{I}_3 & \sigma_{\theta\theta}^0\mathbf{I}_3 & \tau_{\theta r}^0\mathbf{I}_3 \\ \tau_{xr}^0\mathbf{I}_3 & \tau_{\theta r}^0\mathbf{I}_3 & \sigma_{rr}^0\mathbf{I}_3 \end{bmatrix}. \tag{B.6}$$

The linear and nonlinear strain–displacement matrices, $\mathbf{B}_\mathrm{L}$, $\mathbf{B}_\mathrm{NL}$, are given respectively by

$$\mathbf{B}_\mathrm{L} = \mathbf{H}_1\mathbf{G} = \begin{bmatrix} \partial\mathbf{N}_\mathrm{t}/\partial x & 0 & 0 \\ 0 & \partial\mathbf{N}_\mathrm{t}/r\partial\theta & \mathbf{N}_\mathrm{t}/r \\ 0 & 0 & \partial\mathbf{N}_\mathrm{t}/\partial r \\ \partial\mathbf{N}_\mathrm{t}/r\partial\theta & \partial\mathbf{N}_\mathrm{t}/\partial x & 0 \\ \partial\mathbf{N}_\mathrm{t}/\partial r & 0 & \partial\mathbf{N}_\mathrm{t}/\partial x \\ 0 & \partial\mathbf{N}_\mathrm{t}/\partial r - \mathbf{N}_\mathrm{t}/r & \partial\mathbf{N}_\mathrm{t}/r\partial\theta \end{bmatrix}, \tag{B.7}$$

$$\mathbf{B}_\mathrm{NL} = \mathbf{H}_2\mathbf{G}$$

$$= \begin{bmatrix} u_{x,x}\mathbf{N}_{\mathrm{t},x} & u_{\theta,x}\mathbf{N}_{\mathrm{t},x} & u_{r,x}\mathbf{N}_{\mathrm{t},x} \\ [u_{x,\theta}\mathbf{N}_{\mathrm{t},\theta} + (u_x + u_{\theta,\theta})\mathbf{N}_\mathrm{t}]/r^2 & [(u_{\theta,\theta} + u_x)\mathbf{N}_{\mathrm{t},\theta} + (u_\theta - u_{r,\theta})\mathbf{N}_\mathrm{t}]/r^2 & (u_{r,\theta} - u_\theta)\mathbf{N}_{\mathrm{t},\theta}/r^2 \\ u_{x,r}\mathbf{N}_{\mathrm{t},r} & u_{\theta,r}\mathbf{N}_{\mathrm{t},r} & u_{r,r}\mathbf{N}_{\mathrm{t},r} \\ (2/r)u_{x,\theta}\mathbf{N}_{\mathrm{t},x} & (2/r)(u_{\theta,\theta} + u_r)\mathbf{N}_{\mathrm{t},x} & (2/r)(u_{r,\theta} - u_\theta)\mathbf{N}_{\mathrm{t},x} \\ (2/r)u_{x,\theta}\mathbf{N}_{\mathrm{t},r} & (2/r)(u_{\theta,\theta} + u_r)\mathbf{N}_{\mathrm{t},r} & (2/r)(u_{r,\theta} - u_\theta)\mathbf{N}_{\mathrm{t},r} \\ (2/r)u_{x,r}\mathbf{N}_{\mathrm{t},x} & (2/r)u_{x,r}\mathbf{N}_{\mathrm{t},x} & (2/r)u_{r,r}\mathbf{N}_{\mathrm{t},x} \end{bmatrix}. \tag{B.8}$$